Polarization Drift Measurements in Optical Fibers for Long Distance Quantum Communication

Deven Bowman

June 4, 2023

1 Abstract

Polarization drift in optical fibers is studied in the context of developing a polarization drift compensation system for quantum networking atomic systems with > 100 ns long photons. A 26 km fiber, deployed in an urban setting, is used to provide a realistic case study of the polarization drift that will be encountered when trying to achieve long distance entanglement. The rate of polarization drift at one wavelength, 1560 nm, is measured and then compared to measurements of the relative polarization drift between two well separated wavelengths, 1560 nm and 1650 nm.

2 Background

Polarization encoded photonic qubits are a natural candidate for a quantum system that can be used to connect nodes of a quantum network. Photons at telecommunication wavelengths can be sent long distances through optical fibers and the transverse modes of polarization form a true two level system that can act as a qubit. Furthermore, qubit operations can be applied with wave plates, an easy to use and ubiquitous technology. This investigation will explore one of the challenges posed to the implementation of polarization qubits, polarization drift in optical fibers.

In general, the polarization state of light is not preserved through optical fibers. Due to mechanical stresses, temperature fluctuations, and manufacturing defects, optical fibers have random birefringences that may vary with time. This leads to the phenomenon of polarization drift and will contribute systematic uncertainty to measurements of the quantum states sent through the fiber. Therefore, understanding and controlling this is of particular interest for efforts to achieve long-distance quantum communication utilizing polarization-encoded photonic qubits.

A polarization drift control system requires several basic elements. Known polarization reference states need to be sent through the fiber under study. The output states are then measured to drive a programmable polarization controller to apply the correct compensating transformation. A major difficulty is to achieve this without interfering with single photons of the quantum channel at their specific wavelength through the same fiber. Previous attempts have addressed this problem by alternating between transmitting single photons and

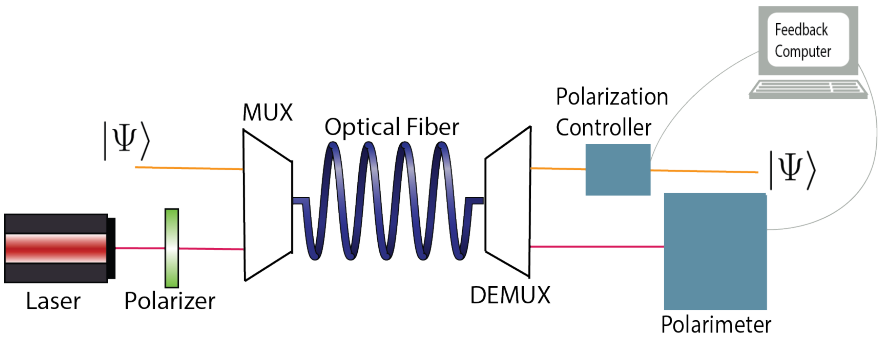

Figure 1: A wavelength division multiplexing polarization drift control system for quantum communication is displayed. One wavelength is used as the quantum channel while polarization reference states are transmitted at a different wavelength.

transmitting bright reference-state light to stabilize the polarization drift [Wu+06]. If the polarization drift occurs on short time scales, the single-channel method requires interrupting the qubit channel frequently. An alternative method, displayed in Figure 1, is to send reference states at a different wavelength and use wavelength division multiplexing (WDM) so that reference states and qubits are simultaneously transmitted for uninterrupted stabilization.

There are two major concerns for a WDM system: isolation between channels and the wavelength dependence of polarization drift. A milliwatt laser at telecommunication wavelengths, reasonable for transmitting reference-state light, produces $\sim 10^{15}$ photons per second. To multiplex this with a single-photon signal requires wavelength filtering with many orders of magnitude of extinction, which can be improved by increasing the wavelength separation, $\Delta\lambda$. But, polarization drift varies with wavelength and, with large enough $\Delta\lambda$, becomes uncorrelated after a time, requiring the transformation matrix relating output states on either channel to be remeasured at repeated intervals [KBA00].

WDM systems have been demonstrated with $\Delta\lambda = 0.8$ nm, small enough to maintain correlation[Xav+08]. To achieve sufficient isolation with such a small separation, Xavier et al. worked with nanosecond length photons and ignored all signals outside of the expected ns-long windows. Atomic systems typically produce photons 10^2 - 10^4 times longer, requiring increased wavelength filtering by these factors, achievable with a larger $\Delta\lambda$. Therefore, an investigation into a polarization drift compensation system using WDM with $\sim 10 - 100$ nm separation between channels is well motivated and the development of such a system will address a barrier to the integration of atomic systems, ideal for quantum memories and processors, into quantum networks.

In this analysis, we will adopt 1° as the important threshold for a polarization drift compensation system to maintain as the upper bound on polarization drift.

Two sets of measurements were performed in this investigation. I measured the magnitude and rate of polarization drift at one wavelength. Next, I measured the relative polarization drift between two wavelengths. The implications of the results to polarization drift compensation systems for quantum networking are discussed and further steps that can be taken to improve this work are suggested.

3 Theory

The Stokes parameter description of polarization uses 4 intensity based metrics to fully describe any full or partially polarized state. Stokes parameters are based solely on observables which makes them the description to use when measuring a polarization state.

$$\vec{S} = \begin{bmatrix} S_0 \\ S_1 \\ S_2 \\ S_3 \end{bmatrix} \tag{1}$$

These 4 parameters in Eq. 1 are calculated with simple intensity measurements. S_0 is the total intensity of the light. S_1 measures the tendency of light to be horizontally polarized(H), $S_1 > 0$, or vertically polarized(V), $S_1 < 0$. S_2 measures the tendency of the light to be linearly polarized in the 45° or −45° directions with $S_2 > 0$ or $S_2 < 0$ respectively. S_3 describes the tendency of the light to be right circularly polarized(R), $S_3 > 0$, or left circularly polarized(L), $S_3 < 0$. A Stokes vector can be written from these parameters to represent any pure or mixed polarization state.

3.1 Pure Polarization States

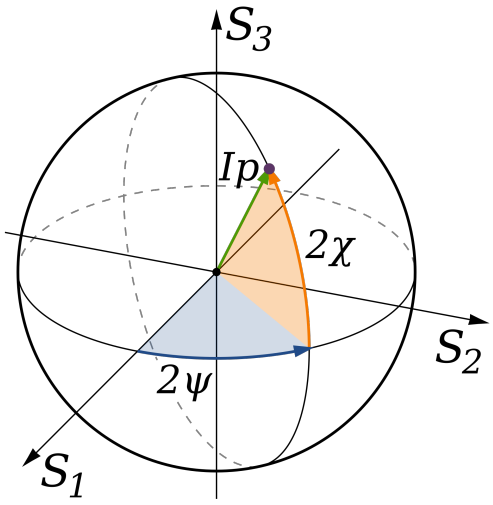

Figure 2: The Poincare sphere and polarization ellipse angles ψ and χ are displayed.

For pure states, we have the property that $S_0^2 = S_1^2 + S_2^2 + S_3^2$. As a result, Stokes vectors are often normalized by S_0 and reduced to a 3D unit vector.

$$\vec{S} = \frac{1}{S_0} \begin{bmatrix} S_1 \\ S_2 \\ S_3 \end{bmatrix} \tag{2}$$

It follows that the set of all pure polarization states can be mapped to a sphere. This mapping is known as the Poincare sphere and is displayed in Figure 2. States on the Poincare sphere can be more concisely represented in terms of two angles.

$$\psi = \frac{1}{2}\arctan\frac{S_2}{S_1}, \psi \in \{0°, 180°\} \tag{3}$$

$$\chi = \frac{1}{2}\arctan\frac{S_3}{\sqrt{S_1^2 + S_2^2}}, \chi \in \{-45°, 45°\} \tag{4}$$

These angles are formulated to describe the polarization ellipse, but 2ψ and 2χ are the spherical coordinate angles on the Poincare sphere. The factors of two represent that the same polarization state is represented when the polarization ellipse is rotated by 180° and when the semi-major and semi-minor axes are swapped.

For the polarization drift and relative drift measurements, we assume that all states are purely polarized since they are generated by laser sources.

4 Single Channel Polarization Drift

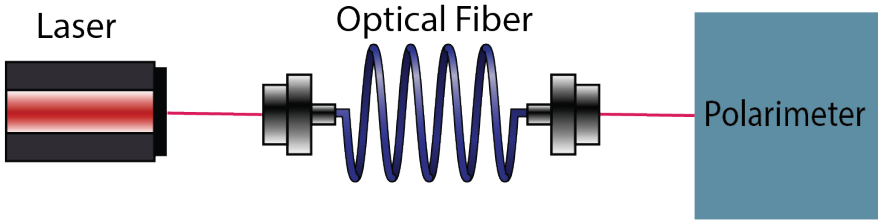

Figure 3: Schematic for the single channel polarization drift measurement.

To study the rate and magnitude of polarization drift in optical fibers, the experimental setup shown in Figure 3 was used where the length and environmental conditions of the optical fiber was varied. In each measurement, a constant reference state was sent through the fiber with a 1560 nm wavelength laser and the polarization was measured $\sim 10,000$ times per second by a polarimeter custom built for this measurement.

4.1 Polarimeter

A six detector Stokes polarimeter was constructed with the schematic depicted in Figure 4. This design uses six intensity measurements that we can relate to the Stokes parameters through a calibration matrix. The photodiode detectors are paired into three detection arms. Light incident on the polarimeter is split into these 3 detection arms by two non polarizing beam splitters, BS_1 and BS_2. Each detection arm has a series of wave plates, depicted as WP_1, WP_2 and WP_3, that apply transformations to the polarization state before reaching a polarizing beam splitter, PBS_1, PBS_2, and PBS_3, that transmits the projection of the state onto the vertical axis and reflects the projection onto horizontal axis. Finally,

a pair of photodiode detectors measures the intensity at each output port of the polarizing beams splitters and produces a voltage signal. While all the PBS's take projections onto the horizontal and vertical, when combined with the preceding wave plates we can realign their projection axes. The Stokes parameters describe the polarization state relative to 3 linearly independent axes. Therefore, we need to set the wave plates to give us 3 linearly independent projection axes for the different detector arms. Furthermore, the farther we can spread the projection axes in Stokes space, the better the resolution we can achieve. To calculate the

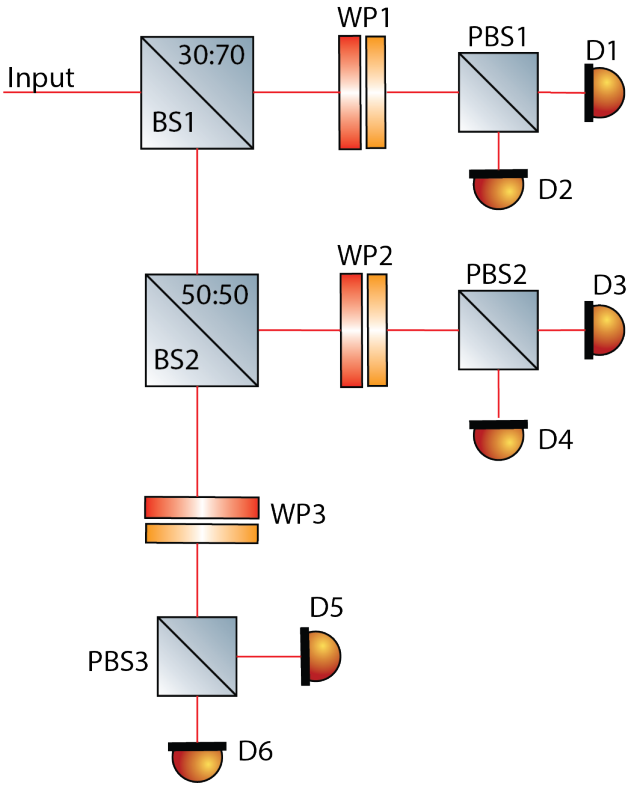

Figure 4: The design for the Stokes Polarimeter uses several beam splitters (BS), waveplates (WP), polarizing beam splitters (PBS), and photodiode detectors (D) to measure the four Stokes parameters.

Stokes parameters from the output voltage signals we generate a matrix from a calibration procedure similar to that presented by Azzam and Lopez[AL89]. For a polarization state with Stokes vector $\vec{S}$, the polarimeter will generate 6 voltages we can write in a vector $\vec{V}$. The two are related by a 6 x 4 matrix $\mathbf{B}$.

$$\vec{V} = \mathbf{B}\vec{S} \tag{5}$$

By generating well defined input polarization states, $\vec{S}$ and then measuring the resulting $\vec{V}$, $\mathbf{B}$ can be determined. This process was performed in 2 stages. First, a linear polarizer was used to generate a series of known linear polarization states. The input polarization state can be calculated with the angle of the transmission axis of the polarizer from vertical θ with

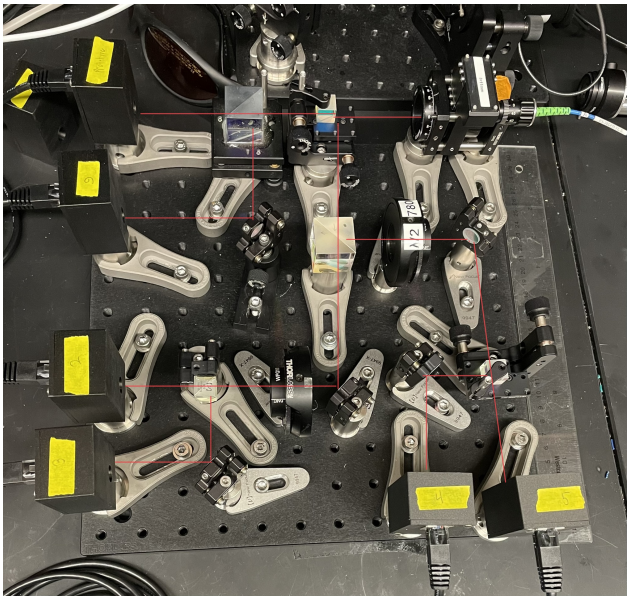

Figure 5: The 6 detector Stokes Polarimeter is displayed with the optical path drawn as a red line for illustration purposes. The light enters the polarimeter from the fiber launch in the top right. The beam is divided into 6 different paths and the resulting intensities are measured by the photodiode detectors in the black boxes.

Equation 6.

$$\vec{S}_{linear} = \begin{bmatrix} S_0 \\ S_1 \\ S_2 \\ S_3 \end{bmatrix} = \begin{bmatrix} 1 \\ -cos(2\theta) \\ sin(2\theta) \\ 0 \end{bmatrix} \tag{6}$$

From equations 5 and 6, the i^{th} component of $\vec{V}$ can be expressed as a linear combination of matrix elements b_{ij}.

$$v_i = b_{i1} - b_{i2}cos(2\theta) + b_{i3}sin(2\theta) \tag{7}$$

I used a linear polarizer with a measured extinction ratio of $> 1000 : 1$ and the orientation of the transmission axis known to $\sim \pm 0.25°$. The linear polarizer was mounted in a motorized rotation mount and rotated continuously through 360° at a rate of 1° per second. The polarimeter recorded measurements at 10,000 Hz. A chi squared fit to the measured v_i was used to determine the b_{ij} matrix elements.

The second stage of the calibration requires input states with some known ellipticity. For this, a procedure, presented in [AL89], was used to account for the error in these input states. First, a linear polarizer and a quarter waveplate were aligned with the transmission axis of the former rotated by 45° from fast axis of the latter. In practice, this produces a nearly circular state. Represented on the Poincare sphere, this state is slightly displaced from one of the poles. Then, by rotating both the linear polarizer and the quarter waveplate by 90°, the input state is rotated by 180 degrees around the north-south axis of the Poincare

sphere. These 2 states are displaced from the pole by a small amount in opposite directions. By averaging the polarimeter measurements associated with each input state, the detector response to a perfect circular state can be attained. By using these calibration measurements, $\mathbf{B}$ was calculated which allows the input states to be calculated from the measured voltage states: $\mathbf{B}^{-1}\vec{V} = \vec{S}$. This calibration matrix, $\mathbf{B}^{-1}$, was applied to the voltage states measured from the linear input states. The results are compared to the theoretical values in Figure 6. Good agreement can be seen between the theoretical curves and the measured curves for the normalized Stokes parameters.

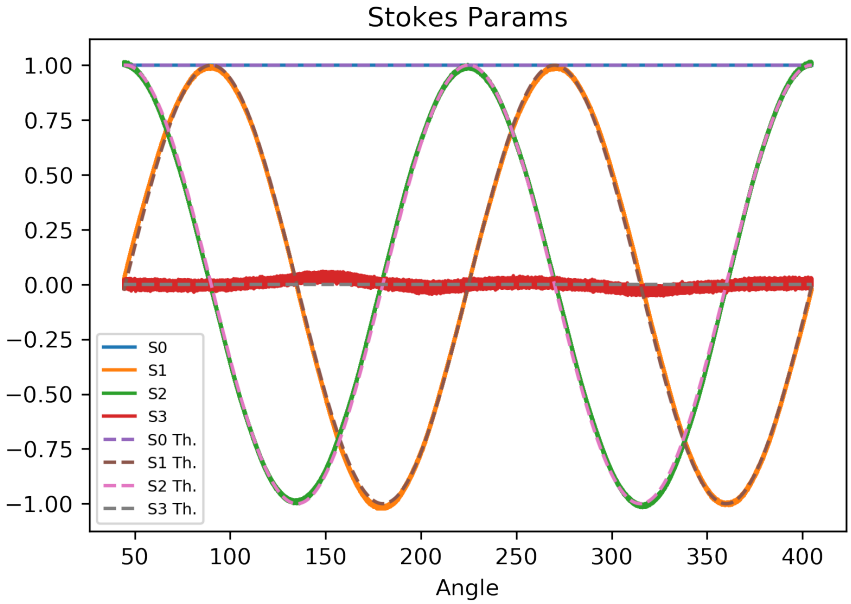

Figure 6: The normalized Stokes parameters are graphed. The measured parameters are solid lines and the theoretical parameters are dotted lines.

4.2 Drift Measurement Procedure

Between the U.S. Army Research Labs(ARL) in Adelphi Maryland and the Atlantic Building at the University of Maryland College Park, there are 2 $\sim$ 13km fiber connections. Currently these fibers are optically connected at ARL. This 26km fiber, deployed in an urban setting, will be the focus of this stabilization system. A $\sim$ 2s trace of the polarization data is presented in Figure 8. The polarization state is represented in terms of the angles ψ and χ on the Poincare sphere. A measurement was also taken through a 3 km fiber spool. Measurements were made when the fiber was undisturbed and also when the fiber was forcibly warmed. A trace of the data from the warming trial can be seen in Figure 9. In addition, measurement was made through a fiber connection that stretched across the lab and back to the polarimeter. This was intended to allow for a comparison between the drift in exposed and buried fibers. Only slow drift on the minute time scale was observed in the intra-lab fiber connection. In the final measurement, the polarization drift was measured

with the shortest possible connection between the laser source and the polarimeter to provide a baseline for noise inherent to the laser source and the polarimeter. No drift is perceptible in trace from the direct connection configuration, displayed in Figure 7. As a result, our measurements of the polarization drift will have very low systematic uncertainties.

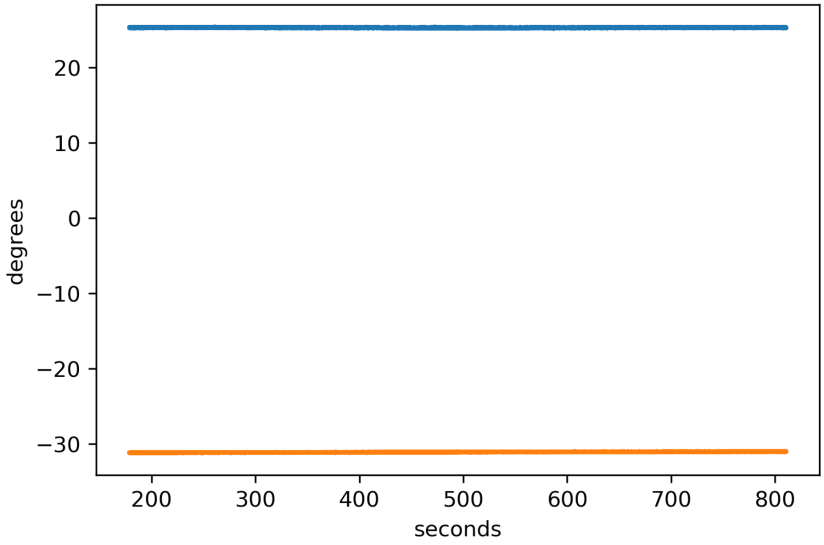

Figure 7: The output polarization state as a function of time is graphed for a constant input state transmitted through a ~ 3 m fiber connection.

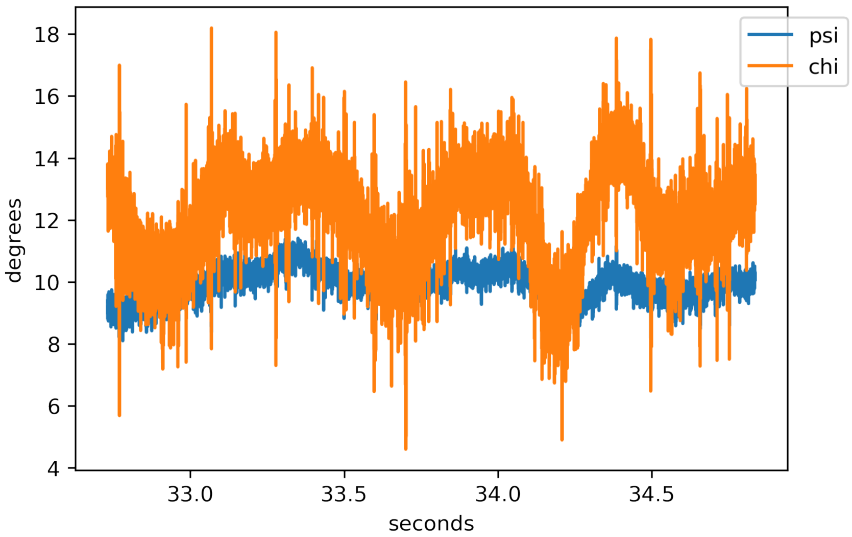

Figure 8: The output polarization state as a function of time is graphed for a constant input state transmitted through the 26km fiber.

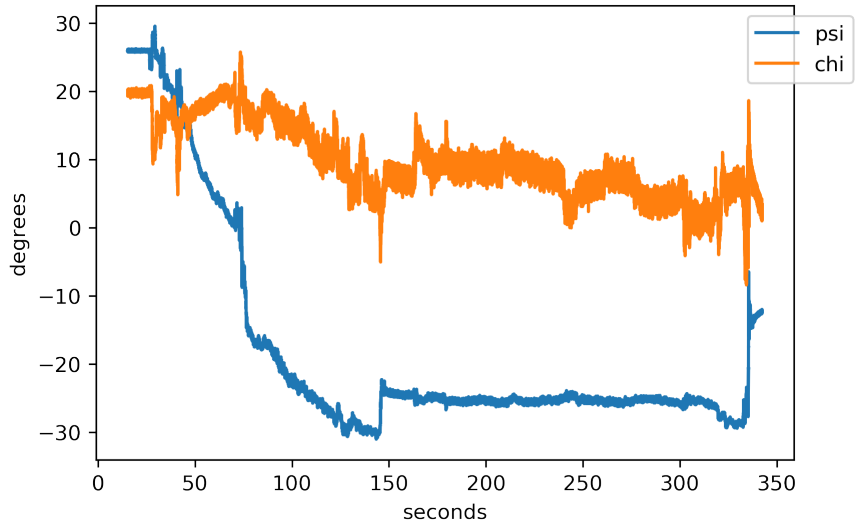

Figure 9: The output polarization state as a function of time is graphed for a constant input state transmitted through a forcibly warmed 3km fiber spool.

4.3 Allan Deviation Analysis

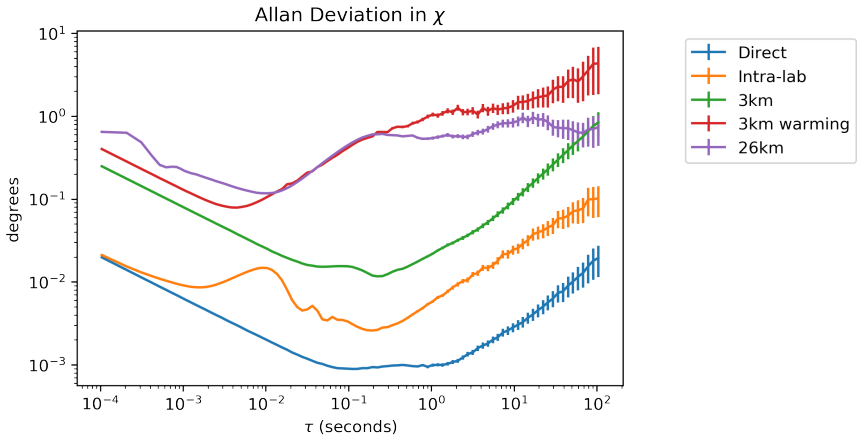

Figure 10: The Allan deviation of χ for light at 1650 nm is graphed for the various fiber conditions.

To quantify the drift, the Allan Variance was employed. The Allan variance was devised to measure the stability of atomic clocks over a range of time scales. In a more general context, it is useful to quantify the stability of a measurement in the presence of noise processes. The Allan variance is calculated with equation 8.

$$\sigma^2(\tau) = \frac{1}{2}\left\langle(\bar{y}_{n+1} - \bar{y}_n)^2\right\rangle = \frac{1}{2(N-1)}\sum_{i=1}^{N-1}(\bar{y}_{n+1} - \bar{y}_n)^2 \tag{8}$$

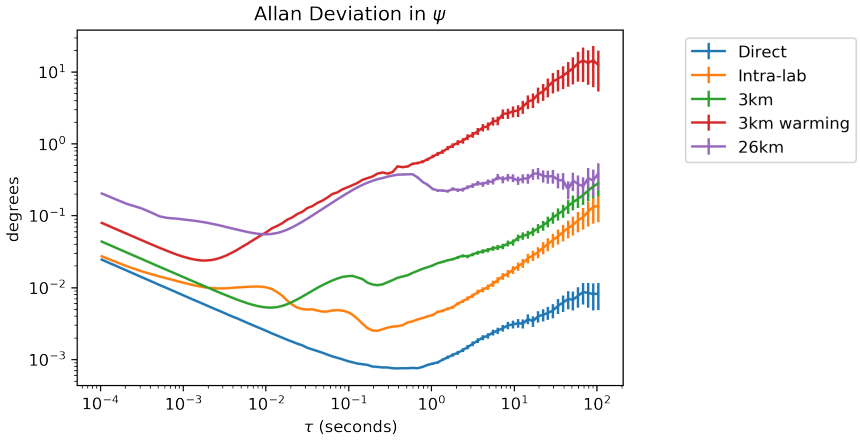

Figure 11: The Allan deviation of ψ for light at 1650 nm is graphed with various fiber conditions.

The data is divided into N consecutive windows of duration τ. The measurements are average within these windows to produce $\bar{y}_n$, for n$^{\text{th}}$ window. The squared difference between $\bar{y}_n$ and $\bar{y}_{n+1}$ is averaged for all N averaged measurements to calculate σ^2. With a polarization drift control system measuring and compensating on a time scale τ, we can expect the polarization drift in the fiber to contribute, on average, systematic uncertainties to the qubit channel of order σ. Figure 10 and 11 display σ for each angle over a range of τ from 0.1ms to 100s for the various fiber conditions. The uncertainty in the Allan deviation measurements depends on the type of noise, but it can be well approximated by $\pm\frac{\sigma}{\sqrt{N+1}}$ where variances between N+1 $\bar{y}$ are averaged [RH08].

In all configurations, σ initially decreases. This reflects that the dominant source of noise is random fluctuations from a static distribution. In this range, averaging for longer τ reduces the deviation. Beyond a certain τ, the deviation increases due to noise resembling a random walk process. The measurements of the 26 km fiber show that the deviation reaches a minimum at $\tau_{min} = 0.01 \pm 0.0015$ s with $\sigma_{min} = 0.1$ degrees for χ. The uncertainty in τ was determined by the spacing between the τ_{min} and the adjacent data points. The Allan deviation was calculated at τ values chosen to be roughly logarithmically spaced at integer multiples of the polarimeter's sample period. A finer spacing of τ values around τ_{min} can be chosen to reduce the uncertainty, but we are primarily interested in establishing the order of magnitude of the time scale of polarization drift. For this τ, N is large giving uncertainty estimate for σ_{min} of $\pm 8 * 10^{-6}$ for σ, far below the needs of this investigation. Therefore, an optimized polarization drift compensation system should drive a polarization controller with measurements of the drift averaged over ~ 10 ms windows. This will allow for polarization drift to be maintained below 1° on the qubit channel.

5 Two Channel Relative Polarization Drift

The same input polarization state at two different wavelengths will, in general, transform through the optical fiber to distinct output states for each wavelength. The relationship between these two output states is expected to vary with time, resulting in relative polarization drift. To measure the relative polarization drift between wavelengths, we need to determine the transformation matrix that relates the output states at either wavelength. Two polarization states were sent through the fiber at each wavelength and the output states were measured. The output states were used to calculate the transformation matrix. Sequential measurements of this matrix allow us to determine the time scales over which polarization drift at either wavelength is correlated.

The polarization transformation induced by the optical fiber can be described as a matrix equation.

$$\mathbf{T}^{\lambda \mathrm{j}} \vec{S}_i^{\lambda_j} = \vec{T}_i^{\lambda_j} \tag{9}$$

$\mathbf{T}$ is the 3x3 transformation matrix of the fiber, $\vec{S}$ is an input polarization state to the fiber, $\vec{T}$ is an output state, and $i \in \{1,2,3\}$, $j \in \{1,2\}$ with i indexing the polarization states and j indexing the wavelengths. By choosing linearly independent input states, $\{s_i^{\lambda_j}\}$ and $\{t_i^{\lambda_j}\}$ form bases for the output and input spaces. We can choose the input basis states to be $\vec{S}_1^{\lambda_j}$, $\vec{S}_2^{\lambda_j}$, and $\vec{S}_1^{\lambda_j} \times \vec{S}_2^{\lambda_j}$ where states 1 and 2 are orthonormal and $\times$ denotes the vector cross product. Since polarization transformations correspond to rotations on the Poincare Sphere, $\mathbf{T}^{\lambda_j}(\vec{S}_1^{\lambda_j} \times \vec{S}_2^{\lambda_j}) = \vec{T}_1^{\lambda_j} \times \vec{T}_2^{\lambda_i}$ because $\mathbf{T}^{\lambda_j}$ preserves lengths and angles between vectors. Therefore, only $\vec{T}_1^{\lambda_j}$ and $\vec{T}_2^{\lambda_j}$ need to be measured at either wavelength to uniquely determine three output states at either wavelength. Then, the transformation matrix between wavelengths can then be calculated.

$$\vec{T}_i^{\lambda_2} = \mathbf{M} \vec{T}_i^{\lambda_1} \tag{10}$$

Equation 10 implies the following relation.

$$\mathbf{B} = \mathbf{M}\mathbf{A} \tag{11}$$

Where the $\mathbf{A}$ and $\mathbf{B}$ matricies are defined as follows.

$$\mathbf{A} = \left[\vec{S}_1^{\lambda_1}, \vec{S}_2^{\lambda_1}, \vec{S}_3^{\lambda_1}\right], \mathbf{B} = \left[\vec{T}_1^{\lambda_2}, \vec{T}_2^{\lambda_2}, \vec{T}_3^{\lambda_2}\right] \tag{12}$$

Then $\mathbf{M}$ can be calculated with $\mathbf{A}^{-1}$.

$$\mathbf{M} = \mathbf{B}\mathbf{A}^{-1} \tag{13}$$

The schematic for the experimental setup is displayed in Figure 12. Lasers at 1560 nm and 1650 nm are each split into two beams by fiber couplers. At each wavelength, polarization controller fiber paddles transform the polarization state of one beam to be linearly independent with the other beam. A Bristol fiber optic switch launches each beam through the fiber sequentially and a PAX1000IR2 polarimeter measures the output polarization states. The PAX1000IR2 measures polarization states in terms of two angles χ and ψ, defined earlier in terms of their relation to the Stokes parameters, with ± 0.25 degree uncertainty up to

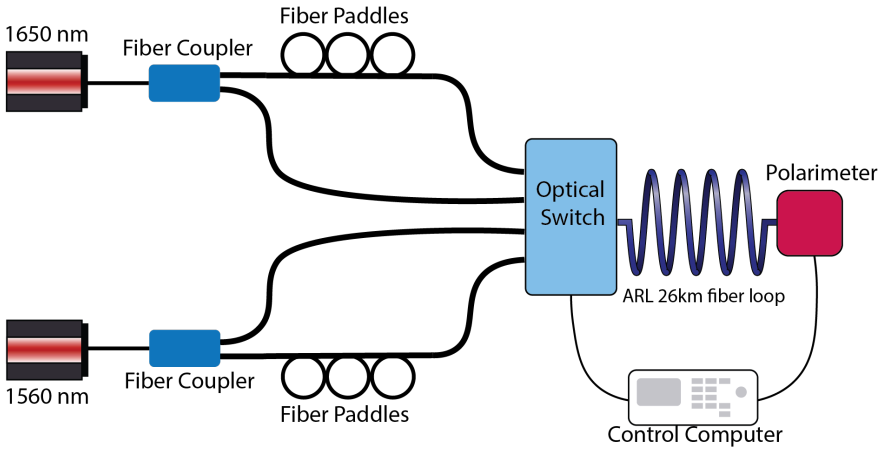

Figure 12: The experimental schematic to measure relative polarization drift at 1560 nm and 1650 nm is displayed.

a sample rate of 400 Hz. The PAX1000IR2 was used, instead of the Stokes polarimeter, since it was easier to work with at multiple wavelengths and the speed of the switch was much slower, no longer necessitating the need for ultra-fast polarization measurements. The optical switch is rated to switch in < 5 ms with a switching frequency of 30 Hz. In practice, switching between channels every 150 ms was the fastest achievable rate due to unpredictable latency in either the switching or polarization measurement acquisition. With four channels to switch to, $\mathbf{M}$ was measured at every 0.6 s. The experiment was controlled by a Python script that communicated with the optical switch and the polarimeter through serial. Data was collected for 30 minutes.

From the measurements of χ and ψ, it was natural to express the states as normalized Stokes Vectors on the Poincare sphere. In this representation, the $\mathbf{M}$ is a 3x3 rotation matrix. Therefore, it can be fully described by an axis of rotation $\vec{n}$ and a rotation angle θ. Both of these can be determined from the eigenvalues and eigenvectors of the matrix. The eigenvalues are $1, e^{i\theta}$, and $e^{-i\theta}$. The eigenvector with eigenvalue 1, $\vec{V_{real}}$, is parallel to the rotation axis and $\cos(\theta)$ is the real part of either complex eigenvalue, allowing for determination of θ. $\vec{V_{real}}$ was normalized to be equal to $\vec{n}$ up to a sign. The polarization states and θ, were observed to vary smoothly. Therefore, the sign of $\vec{n}$ was chosen to maintain continuity. Since $\vec{n}$ is also a point on the Poincare sphere, it can be concisely represented in terms of two angles, ψ and χ, giving us a total of three angles that encode the $\mathbf{M}$.

An Allan deviation analysis was performed on these three angles to allow for a comparison to the single channel polarization drift. The Allan deviation is expected to present similar trends to that of the single channel drift. For sufficiently small τ, the $\mathbf{M}$ will be measured much faster than the rate at which it drifts. In this range, the deviation will decrease as measurements are averaged over longer τ. At some characteristic time scale τ_{min}, the random walk drift will begin to increase the deviation for longer averaging windows. Therefore, τ_{min} for single channel and two channel relative drift allow for a comparison of the time scales of drift. The Allan deviation results are displayed in Figure 13 for 0.6s $< \tau <$ 600s. The

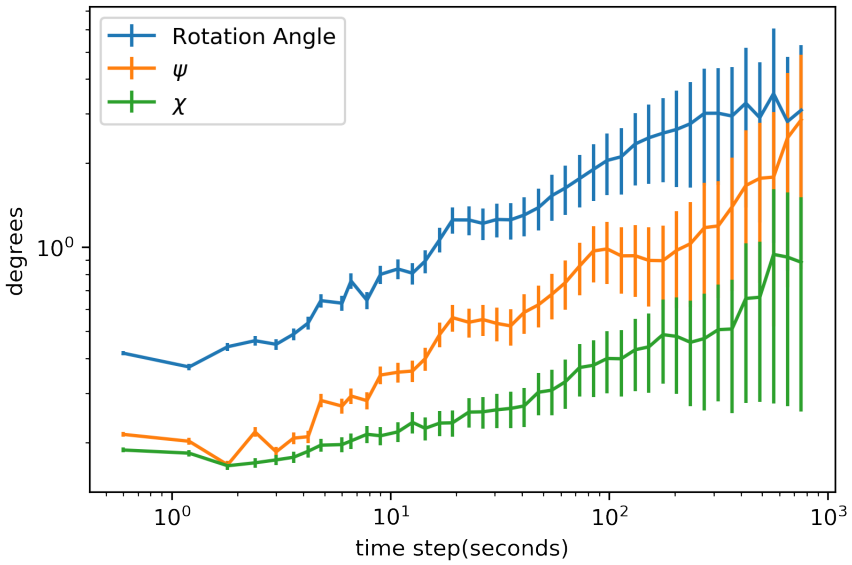

Figure 13: The Allan deviation of the two angles that define the rotation axis, χ and ψ, and the rotation angle. These quantities describe relative drift between channels at 1560 nm and 1650 nm.

lower bound is set by the sample rate of the measurement and the upper bound was limited by the duration of the data taking. The Allan deviation of all three angles present local minima at $\tau_{min} =\sim 2$ s but this approaches the sample rate of the measurement. Therefore, the data provides a coarse set of τ from which we can calculate σ. However, it is clear that the increasing slope characteristic of random-walk noise begins on the several second time scale. For these time scales, the average deviation between rotation angles is ~ 0.4 degrees and, for ψ and χ, is 0.2 degrees. At $\tau = 2$ s, the sum of all angles is less than 1°, suggesting there is a parameter regime that the WDM system in Figure 1 could operate and maintain less than 1° polarization drift on the qubit channel.

6 Results

It is clear that the polarization drift at 1560 nm and 1650 nm are not correlated for long times. The transformation matrix between the output states at either wavelengths varies in time. However, this variation may be slow enough to allow for a dual channel WDM system to be implemented. Polarization was found to drift on the 0.1° scale over the 10 ms time scale. By comparison, the relative drift between two channels, in terms of the drift of the three angles that define the transformation matrix, was found to drift by tenths of a degree over seconds. A drift control system could take advantage of the correlation between wavelengths for short times to reduce the rate at which the qubit channel needs to be interrupted. In this system, the transformation matrix between the control reference state channel and the qubit channel could be measured every several seconds. In between these measurements, the polarization drift can be continuously measured on the reference state channel to allow for

polarization compensation of the qubit channel. During this window, there will be relative drift between the two channels which will increase the systematic uncertainties on the qubit channel. This investigation shows that these additional uncertainties can be expected to be $< 1^\circ$ on average.

7 Continuing Work

The two channel relative polarization drift measurement will provide more definitive results with a faster sample rate for the measurement. This experiment was limited by unpredictable latency in either the response of the optical switch or the PAX1000IR2 to commands.

I am working on a measurement that should identify either the switch or the polarimeter as the issue. A laser will be sent into one of the ports of the switch while the rest will be dark. A function generator will create TTL pulses to drive the switch between the light and dark channels. A photodiode will measure the output signal on an oscilloscope that is also synchronized with the TTL signal. Varying latency in the switching time will generate a signal on the oscilloscope that is unstable when the trigger is set to the TTL signal.

The sample rate will increase by a factor of four by optimizing the current hardware. This will allow us to probe smaller τ for the relative drift and increase the resolution near τ_{min}.

References

[AL89] R. M. A. Azzam and Ali G. Lopez. "Accurate calibration of the four-detector photopolarimeter with imperfect polarizing optical elements". In: *J. Opt. Soc. Am. A* 6.10 (Oct. 1989), pp. 1513–1521. DOI: 10.1364/JOSAA.6.001513. URL: http://opg.optica.org/josaa/abstract.cfm?URI=josaa-6-10-1513.

[KBA00] Magnus Karlsson, Jonas Brentel, and Peter A. Andrekson. "Long-term measurement of PMD and polarization drift in installed fibers". In: *Journal of Lightwave Technology* 18.7 (2000), pp. 941–951. DOI: 10.1109/50.850739.

[Wu+06] Guang Wu et al. "Stable polarization-encoded quantum key distribution in fiber". In: (2006). DOI: 10.48550/ARXIV.QUANT-PH/0606108. URL: https://arxiv.org/abs/quant-ph/0606108.

[RH08] William Riley and David Howe. *Handbook of Frequency Stability Analysis*. en. July 2008. URL: https://tsapps.nist.gov/publication/get_pdf.cfm?pub_id=50505.

[Xav+08] G. B. Xavier et al. "Full polarization control for fiber optical quantum communication systems using polarization encoding". In: *Opt. Express* 16.3 (Feb. 2008), pp. 1867–1873. DOI: 10.1364/OE.16.001867. URL: https://opg.optica.org/oe/abstract.cfm?URI=oe-16-3-1867.